Front. Energy 2021, 15(4): 860–871
https://doi.org/10.1007/s11708-021-0744-1

RESEARCH ARTICLE

Zhimin QIU, Daogang LU, Jingpin FU, Li FENG, Yuhao ZHANG

Experimental study of primary and secondary side coupling natural convection heat transfer characteristics of the passive residual heat removal system in AP1000

Abstract Passive residual heat removal heat exchanger (PRHR HX), which is a newly designed equipment in the advanced reactors of AP1000 and CAP1400, plays an important role in critical accidental conditions. The primary and secondary side coupling heat transfer characteristics of the passive residual heat removal system (PRHRS) determine the capacity to remove core decay heat during the accidents. Therefore, it is necessary to investigate the heat transfer characteristics and develop applicable heat transfer formulas for optimized design. In the present paper, an overall scaled-down natural circulation loop of PRHRS in AP1000, which comprises a scaled-down in-containment refueling water storage tank (IRWST) and PRHR HX models and a simulator of the reactor core, is built to simulate the natural circulation process in residual heat removal accidents. A series of experiments are conducted to study thermal-hydraulic behaviors in both sides of the miniaturized PRHR HX which is simulated by 12 symmetric arranged C-shape tubes. For the local PRHR HX heat transfer performance, traditional natural convection correlations for both the horizontal and vertical bundles are compared with the experimental data to validate their applicability for the specific heat transfer condition. Moreover, the revised natural convection heat transfer correlations based on the present experimental data are developed for PRHR HX vertical and lower horizontal bundles. This paper provides essential references for the PRHRS operation and further optimized design.

Received Sept. 25, 2020; accepted Feb. 23, 2021; online May 15, 2021

Zhimin QIU, Daogang LU, Jingpin FU, Li FENG, Yuhao ZHANG (✉)
School of Nuclear Science and Engineering, North China Electric Power University, Beijing 102206, China; Beijing Key Laboratory of Passive Safety Technology for Nuclear Energy, Beijing 102206, China
E-mail: zhangyuhao@ncepu.edu.cn

Special Issue: Innovative Nuclear Energy Technology

Keywords passive residual heat removal heat exchanger (PRHR HX), C-shape tube, revised heat transfer correlations, coupled natural convection

1 Introduction

To enhance the safety of nuclear reactors, passive safety systems which rely on natural forces to achieve safety functions have been explored and widely applied in the advanced reactors of AP1000 and CAP1400. Being one of the important components of passive safety systems, passive residual heat removal system (PRHRS) removes the core decay heat to the heat sink in-containment refueling water storage tank (IRWST) when natural circulation is formed in density contrast between the PRHRS and RCS in critical accidental conditions. The prototype of the PRHR HX composing 689 heat transfer tubes C-shape bundle locates at one side of the IRWST [1]. Due to its complex structure and special arrangement, the heat transfer process is so complicated that its heat transfer mechanisms are not very clear yet. Thus, in-depth research on details of the heat transfer process and behaviors of the natural circulation is essential to improve its practical applicability.

In previous research, several integrated effect experiments such as APEX [2], ROSA [3], etc. which adopt PRHR system were performed to verify the safety of advanced reactors in severe accidents. The PRHR HX model equipment works as an important part in those test facilities. Its heat transfer capacity and action were mainly tested and studied to confirm the passive safety characteristics of the designed advanced reactors. In recent research, an increasing number of PRHR HX separate-effects experiments were performed to investigate local thermal-hydraulic behaviors of the C-shape tubes bundle. Men

et al. [4] conducted a series of experiments to investigate the natural convection heat transfer characteristics of a single C-tube, and compared traditional heat transfer correlations for the tube outside and inside heat transfer with the experimental data to find the best-fit correlation. Lu et al. [5] and Zhang et al. [6] built an overall scaled-down IRWST and PRHR HX model, which consisted of 12 electrical heating rods bundle located at one side of the IRWST, to investigate the natural convection and pool-boiling heat transfer mechanisms of C-shape rods bundle in different stages during its operation. Moreover, they compared traditional correlations for different bundle sections and heat transfer mechanisms with the experimental data to validate their applicability for system analysis of the PRHRS. Furthermore, they proposed the revised correlations based on the data to match the specific operating conditions of PRHR HX. Tao et al. [7] investigated the transient single-phase thermal hydraulics of PRHR HX by a miniature model consisting of 6×7 C-shape tube bundle, by performing both experiments and numerical simulations. On the one hand, they compared traditional correlations published in literatures with the experimental values to find the best-fit one for the specific heat transfer condition. On the other hand, they validated numerical simulation results by experiments and obtained more details of flow patterns and local heat transfer characteristics. Liu et al. [8] explored the heat transfer of PRHR HX by a test facility of C-shape tubes bundle immerged in a water tank. They found three heat transfer regions during the heating process on the outer tube surface: natural convection region, transition region, and saturation boiling region. Besides, they analyzed the correlations for different regions in the said paper and their previous work [4]. Kang [9] investigated the effects of different major parameters including surface roughness, tube diameter, wall superheat, and dimensionless tube length, which were introduced into pool boiling heat transfer behaviors of a vertically mounted tube. Additionally, he obtained an empirical correlation for pool boiling heat transfer to quantify the tube length effect by using the experimental data.

In the present paper, both the primary and secondary side coupling heat transfer characteristics of PRHR HX were experimentally studied. The primary side of the PRHR HX model was added to the test facility which was built in Refs. [5,6]. The classical correlations for natural convection in the secondary side of PRHR HX were compared with the present experimental data. Moreover, the natural circulation behaviors of the primary side and local single-phase heat transfer characteristics for different parts of C-shape tubes bundle were also analyzed. Furthermore, the revised heat transfer correlations for PRHR HX lower and vertical bundles under natural convection condition were developed.

2 Experimental setup and measurements

2.1 Experimental setup and test procedure

The test facility was built based on the scaling analysis in Ref. [5], with some modifications made for the present study. In the present experimental setup, 12 symmetric arranged C-shape tubes were installed to replace the electrical heating rods bundle and a simulator of the reactor core was used to heat the fluid in the primary side of the

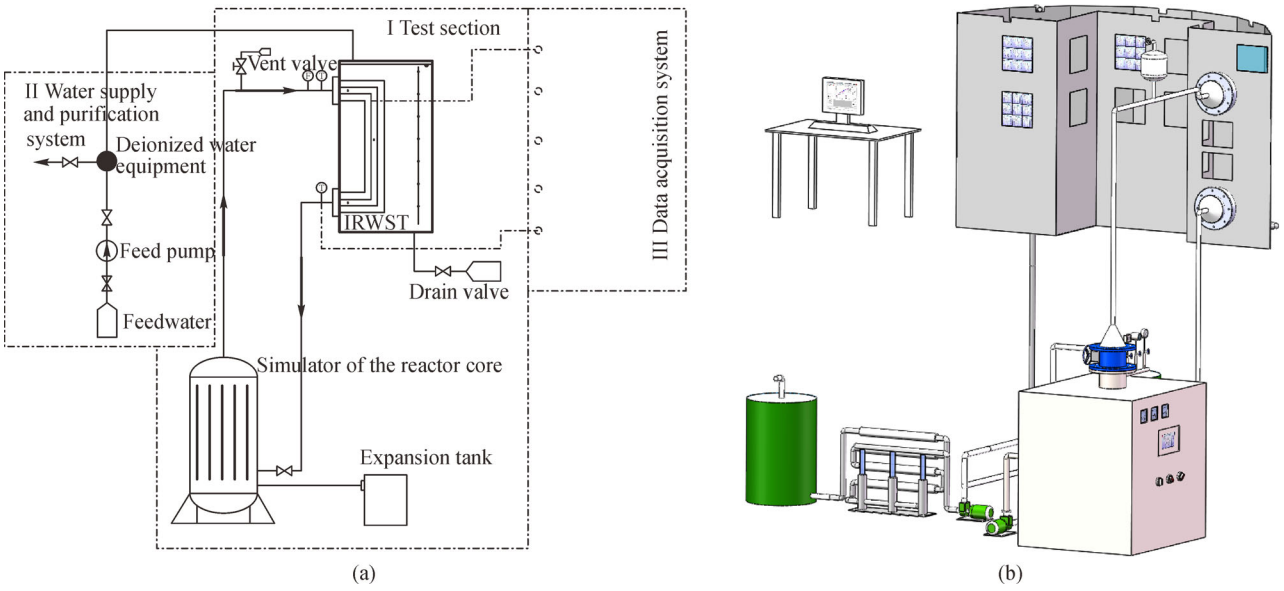

Fig. 1 Schematic of experimental setup.
(a) Arrangement of experimental setup; (b) model of experimental setup.

PRHR HX model. The schematic illustration of the test apparatus is shown in Fig. 1.

The experimental setup consists of the test section, a water supply and purification system, and a data acquisition system. The key parameters of the prototype and the test apparatus are listed in Table 1. The IRWST model and PRHR HX model are elevated to about 2.5 m high for the simulation of natural circulation behaviors in the primary side, whose dimensions are designed by scaling analysis results. The simulator of the reactor core is mounted on the ground, whose major structure is a cylinder with a height of about 1.3 m and a diameter of 1.2 m. Five groups of heating rod whose length is 1.1 m are vertically placed in the cylinder by fixing on the top annularly. Each group has a rated power of 64 kW and thus the total power of the heating rod amounts to 320 kW. The major parameters are listed in Table 2. The IRWST model is scaled down to approximately 3.75 m × 1.5 m × 2.2 m, and its irregular shape is kept the same as the prototype. The PRHR HX model comprises of 12 C-shape tubes bundle located at one corner of the IRWST, which is connected to the simulator of the reactor core. The bundle is divided into the lower horizontal section, the vertical section, and the upper horizontal section according to their specific heat transfer characteristics. The vertical section and the horizontal sections are scaled down to about 1.4 m, and 0.7 m, respectively. When the natural circulation forms, the hot fluid heated in the simulator of the reactor core is driven by the buoyancy and gets into C-shape tubes bundle to transfer the heat to the water in the IRWST model through tubes. The primary and secondary side coupling effects determine the heat transfer performance directly. Then the cooled fluid returns to the simulator to be heated again to simulate the long-term cooling process. The maximum operating pressure is up to 1.6 MPa to prevent the primary side fluid from being vaporized.

Table 1 Comparison of parameters between prototype and experimental model

Items	Prototype parameters	Scaled model parameters
IRWST length in lateral direction/m	About 36	3.75
IRWST length in height direction/m	8	2.2
PRHR HX tubes number	689	12
Outer diameter of heat transfer tube/mm	19	19
Inner diameter of heat transfer tube/mm	15.75	15.75
Pitch to diameter ratio	1/2	1/2

Table 2 Parameters of simulator of reactor core

Items	Parameters
Length in height direction/m	1.3
Length in lateral direction/m	1.2
Length of the heating rod/m	1.1
Diameter of the heating rod/m	0.125
Group number of the heating rod	5
Heat power/kW	320

At the beginning of the test, the primary side and IRWST model are filled with purified water and the simulator of the reactor core operates at full power rate to raise the fluid temperatures in both sides to the preset values. Meanwhile, a mixing pump is used to mix the fluid in the tank. During the heating process, natural circulation is formed with an initial velocity of zero. After the fluid reaches the preset temperatures, the simulator is set at the preset power rate and operating pressure, and the mixing pump stops working to circulate the water. Then, the formal experimental test can be performed and all the experimental parameters can be obtained by measurements and the data acquisition system. The main test condition parameters are summarized in Table 3.

In this paper, the heat power, water level, and pressure in the primary side are set at a rate power of 60 kW, 2.2 m, and 0.6 MPa respectively, the condition of which are analyzed in depth. The initial temperature of the fluid in the bulk region is ambient temperature (20°C) without circulation by the pump. When the heat power is 120 kW or higher, the heat transfer capacity of the heat exchanger is lower than the power, causing a continuously increase of the pressure. To keep the same pressure in the test, the power of the simulator changes automatically according to the setup and actual parameters.

2.2 Measurements

The schematic diagrams of the temperature measurements in the test section are demonstrated in Figs. 2 and 3. According to the local flow structures, the measured area is divided into three parts.

The first part is the tubes inner flow channels. Thirty-five thermocouples are placed in five selected tubes C1–C5 through two small holes made at the inlet and outlet flanges, and two holes are sealed by the sealing device. As can be noticed in the horizontal and vertical bundle cross sections in Fig. 2(a), each row has at least one selected tube to measure the temperature distribution in different regions. To pay close attention to the bundle effects, two of the four tubes, i.e., C3 and C4, in the central region are chosen to study the heat transfer characteristics. As can be observed in Fig. 2(b), the selected tube C2 has seven temperature metrical points in different parts and the other selected tubes also have the same number of metrical points. The first and third thermocouple metrical points of the five selected tubes are set within the same horizontal plane and vertical plane respectively, which are the same as the other metrical points. Those thermocouples are not fixed in the tubes, whose positions are decided by their lengths of sheathed part extending in the tubes. For the

Table 3 Parameters of test condition

No.	Pressure/MPa	Saturation temperature/°C	Power/kW	Initial water temperature in IRWST/°C	Initial water level in IRWST/m
1	0.6	158.8	60	20	2.2
2	1.2	188.0	60	20	2.2
3	1.2	188.0	120	50	2.2
4	0.6	158.8	120	50	2.2
5	0.6	158.8	120	70	2.2
6	1.6	201.4	120	70	2.2
7	0.6	158.8	160	50	1.5
8	1.2	188.0	160	70	1.5
9	1.2	188.0	160	50	1.0
10	0.6	158.8	160	50	1.0
11	1.2	188.0	160	50	0.6
12	1.6	201.4	160	70	0.6

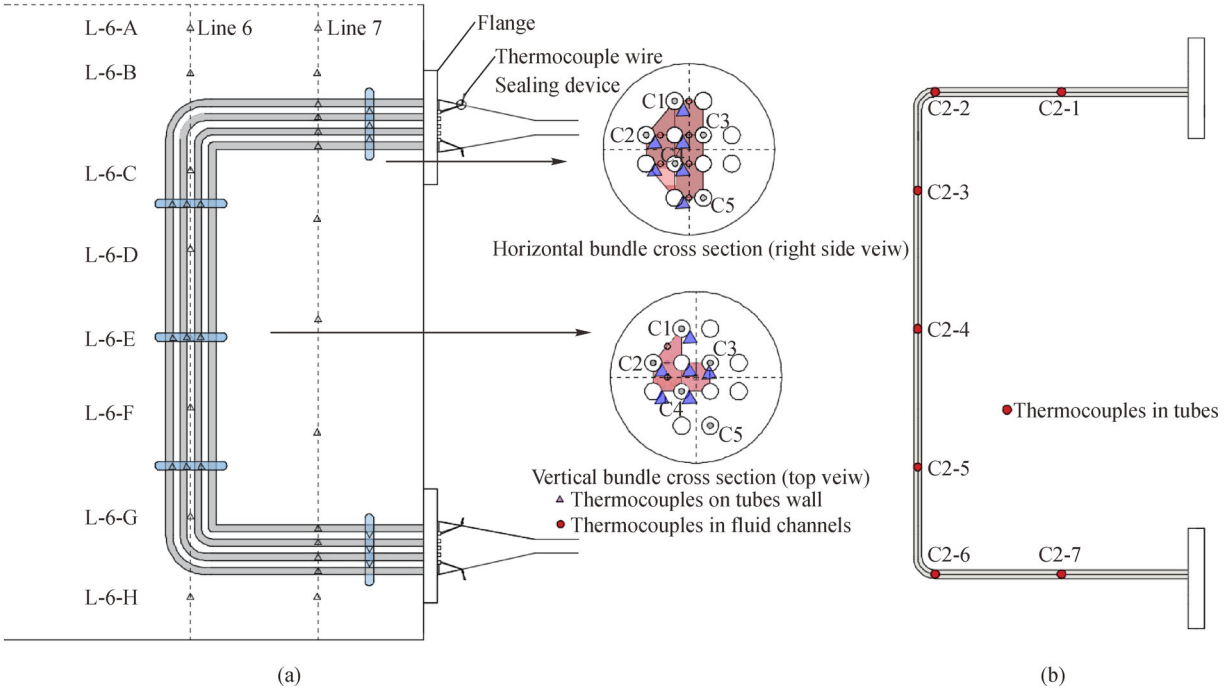

Fig. 2 Temperature measurements.
(a) Local temperature measurements matrix; (b) thermocouple arrangement in C2 tube.

reasons of thermocouple allocation in tubes, the thermocouples are placed to measure the variation of the fluid temperature along the direction of the flow so that the rates of heat transfer in different parts can be calculated.

The second part is the outside wall of the tubes and the region between tubes. As can be seen in Fig. 2(a), the thermocouples on the outer wall of the tubes and in the fluid sub-channels in the upper and lower horizontal bundles are set within two horizontal planes. More details are displayed in the horizontal bundle cross section, where six thermocouples are carefully welded on the left half of the bundle and another six thermocouples are placed within the different types of fluid sub-channels. Considering the influence of the upper flow, there are six different types of flow channels in the horizontal part. For the vertical bundle, three vertical planes are selected to place the temperature metrical points because there are only three different types of flow channels. From the vertical bundle cross section, six thermocouples are set on the outside wall and three thermocouples are set in three different types of fluid sub-channels. The thermocouples in the second part are set in the middle of the two metrical

points in the tube according to the positions of the thermocouples to calculate the heat transfer coefficients (HTCs) and obtain the physical properties of the fluid surrounding the tubes on the secondary side.

The last part is the large volume IRWST region. More than 60 T-type stainless steel sheathed thermocouples are fixed on 7 stainless rods, which are vertically installed in the tank to obtain the temperature distribution along both the lateral and height directions. Eight or 14 thermocouples as thin as 0.5 mm at different heights are set on monitoring Lines 1–6, and Line 7 respectively. As can be seen in Fig. 3, the specific positions of the stainless rods and thermocouples in the IRWST are given. In the *xy*-Plot, key monitoring Lines 1–7 are located along the lateral direction in the IRWST. In the *xz*-Plot, eight thermocouples at different heights are set on temperature monitoring Lines 1–5. Since the *x*-coordinates of Lines 3, 6, and 7 are very close to each other, the positions of the thermocouples fixed on Lines 6 and 7 are depicted in Fig. 2(a). The diameters of those thermocouples and rods are so small that they have little effect on flow patterns in the tank. Most of the monitoring lines are located around the tubes bundle to study the local heat transfer characteristics. The flow rate of the primary side fluid is measured by a high precision ultrasonic flow meter located at the inlet and the pressure of the primary side is controlled by the simulator of the reactor core.

A total of 21 visualization windows are set on the tank side wall for the visualization observation and a high-speed camera with a capturing frequency of 1000 FPS is employed to record the transient flow patterns. All the signals of thermal parameters are recorded by the input modules (NI PXIe-4353) with a sampling rate of 5 Hz and analyzed by the Data Acquisition System. In the present experiment, the major measuring sensors are calibrated by the qualified organization. The T-type sheathed thermocouple measuring range is from −200°C to 350°C with a measuring accuracy of 0.4%. The measuring accuracy of the volume flow rate is 0.05%. The uncertainties associated with the direct parameters compose of the sensor direct measurement error and data acquisition error (high accuracy of 0.00625%). As a result, the combined uncertainties for the temperature and flow rate approximately equal 0.4% and 0.05%, respectively.

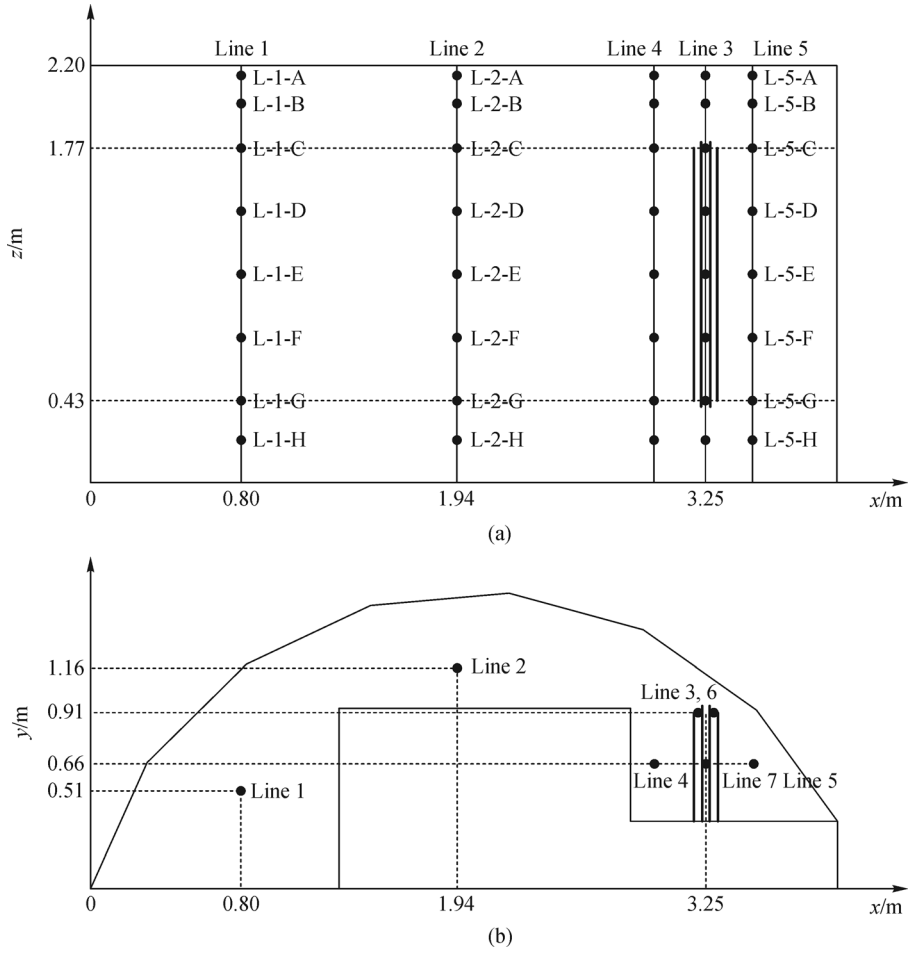

Fig. 3 Key monitoring lines in IRWST and PRHR HX model.
(a) *xz*-plot; (b) *xy*-plot

3 Results and discussion

3.1 Thermal and flow performance in primary and secondary side

For the bulk region besides the PRHR HX model, the temperature distribution is recorded by monitoring points along Lines 1, 2, 4, and 5. As shown in Fig. 4(a), the thermal variation in the bulk region at different times are given and the experimental data measured by the metrical point L-2-A which is out of order are ignored. On the one hand, the values measured by points along one line increase with its height, which validates the temperature thermal stratification existing in the height direction. On the other hand, the values measured at the same elevation on different lines are very close to each other at different times and it seems that there is no obvious thermal differences in the lateral direction although its length is greater than that in the height direction. This phenomenon indicates that the fluid heated by the PRHR HX model flows up under the buoyancy driving force, causing the accumulation of heat and the rise of the fluid temperature in the upper region. The fluid in the lower region remains thermally inactive and its temperature stays in the initial value for a very long time during the heating process.

For the transient temperature measurement of fluid channels between tubes, Figs. 4(b) and 4(c) show the thermal variation in the bulk region along Lines 6 and 7. The temperatures measured by most metrical points on Lines 6 and 7 change greatly. To explain this change, the local temperature measurements matrix is given in Fig. 2 (a). It can be noticed from Fig. 2(a) that the metrical points L-6-C–L-6-G are set between the tubes in the vertical bundle section. Measuring points L-7-C–L-7-F, J–M are placed between the tubes in the upper and lower bundle sections, respectively. As exhibited in Figs. 4(b) and 4(c), the temperature values measured by those points between the tubes in the secondary side scatter in a quiet

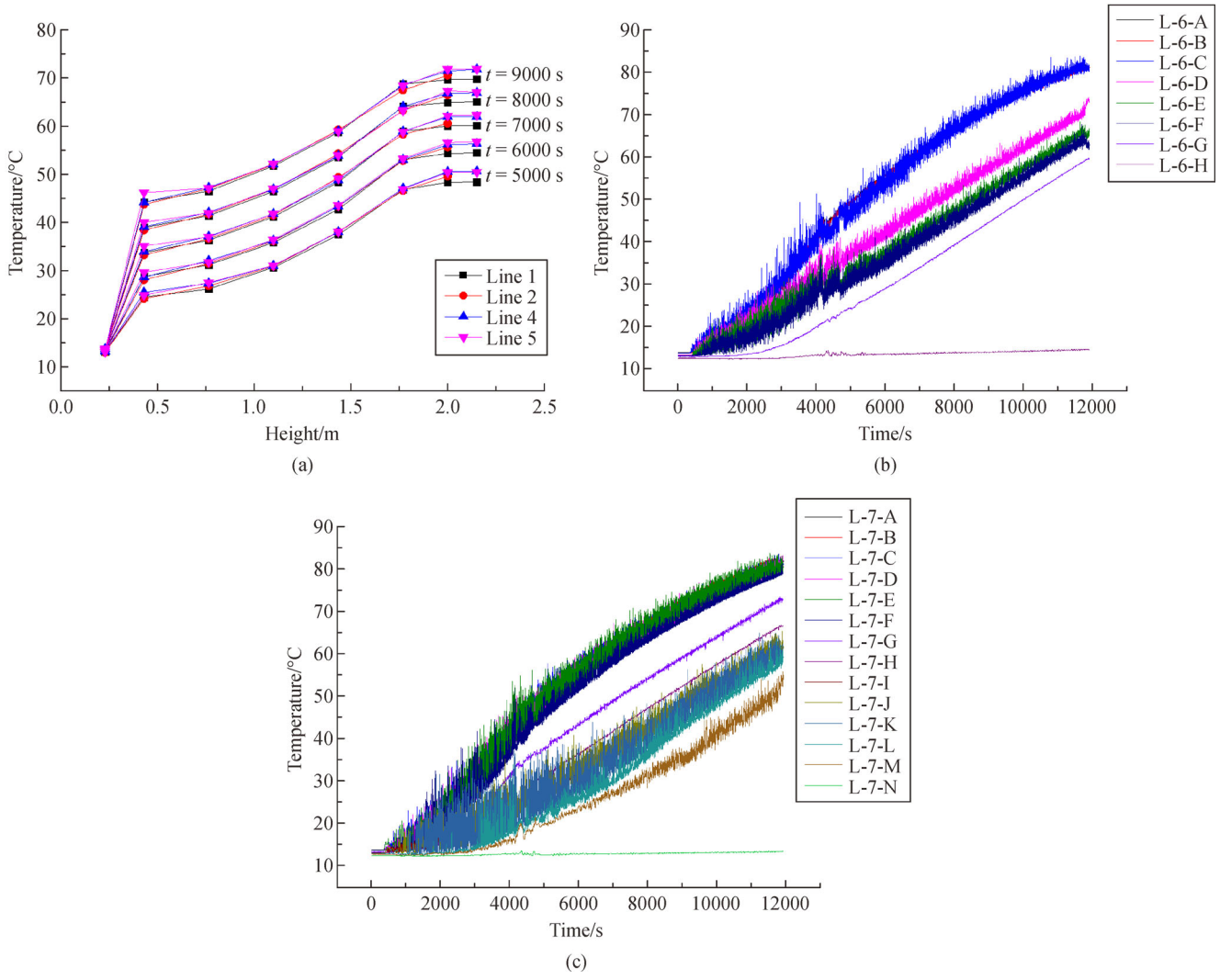

Fig. 4 Thermal variation in bulk region.
(a) Thermal stratification along Lines 1, 2, 4, and 5; (b) transient temperature variation along Line 6; (c) transient temperature variation along Line 7.

larger region than that measured by other points outside the bundle. For the region in the fluid sub-channels between tubes, heat is transferred from the tube wall to the surrounding fluid, causing a decrease of density. The heated fluid will flow upward and then the lower and surrounding cooler fluid occupy the leaving space. The mixture of hot and cool fluid occurs in the region, leading to an obvious temperature oscillation. When the nucleate boiling occurs, the generation and departure of bubbles further enhance the oscillation. For the fluid surrounding the C-shape tubes bundle, the fluctuation in this region is weaker than that in sub-channels, which indicates that the process of heat transfer is mild. For the metrical points L-6-H and L-7-N, the experimental data measured by the two points at the bottom of the IRWST keep the same as the initial value, indicating that the thermal disturbance is small, and heat is mainly transferred by the heat conduction in this region. For points L-7-G–L-7-I, those measuring points are placed between the upper and the lower bundles to measure the temperature distribution. The oscillation of the temperature in the region is not obvious judging from Fig. 4(c). Hence, the temperature variation in the IRWST far away from the C-shape bundle is steady and fierce heat transfer does not happen. The results described above are much the same as those obtained in Ref. [5] where only the secondary side is taken into account. The thermal hydraulic characteristics of the primary side are also elaborated as follows.

To study the thermal hydraulic characteristics in heat transfer tubes, the transient temperature variation in a single tube is recorded by thermocouples in tube flow channels. As depicted in Fig. 5, the temperature of the fluid in the tube remains steady with oscillation within a narrow range and decreases along the flow direction because of the continual cooling down by the cold fluid in the secondary side when the stabilization stage of natural circulation forms. In this stage, the heat produced by the simulator is totally transferred from the primary side to the secondary side, which also validates its capacity to remove the core decay heat in the simulation. As the test proceeds, the temperature drop between C2-1 and C2-7 becomes smaller due to the increase of flow rate in the primary side.

From Fig. 6, the fit curve of the temperature distribution in the single tube is obtained through the temperature measured values. The temperature gradient of any two measuring points is approximately equal to each other.

For the flow performance in the primary side, the fluid flows through the flow channels and the flow performance is unable to be captured by the camera directly. However, the fluid flow rate and temperature in the tubes can be measured by the flow meter and thermocouples, and thus the Reynolds number (Re) is calculated by dividing the kinematic viscosity into the inertial force of the fluid to study the flow condition in the C-shape tube. The results in the range of $Re = 4 \times 10^4$–1.2×10^5 under natural convection condition show that turbulent flow occurs in the tube. It is a typical single-phase forced-convection heat transfer process, for which the refined Dittus-Boelter correlation is applied to evaluate the heat transfer characteristics.

For the flow performance in the secondary side, the heat transfer mechanism changes with the rise of temperature in the secondary side during the heating process. When the temperature of the secondary side is low, no bubbles are produced on the outside wall of the tube and the stage of natural convection occurs. The heat transfer characteristics in this stage are mainly studied in this paper. In this stage, the upper flow is formed by the density contrast with a low velocity, which can be shown by the video shot by the CCD camera.

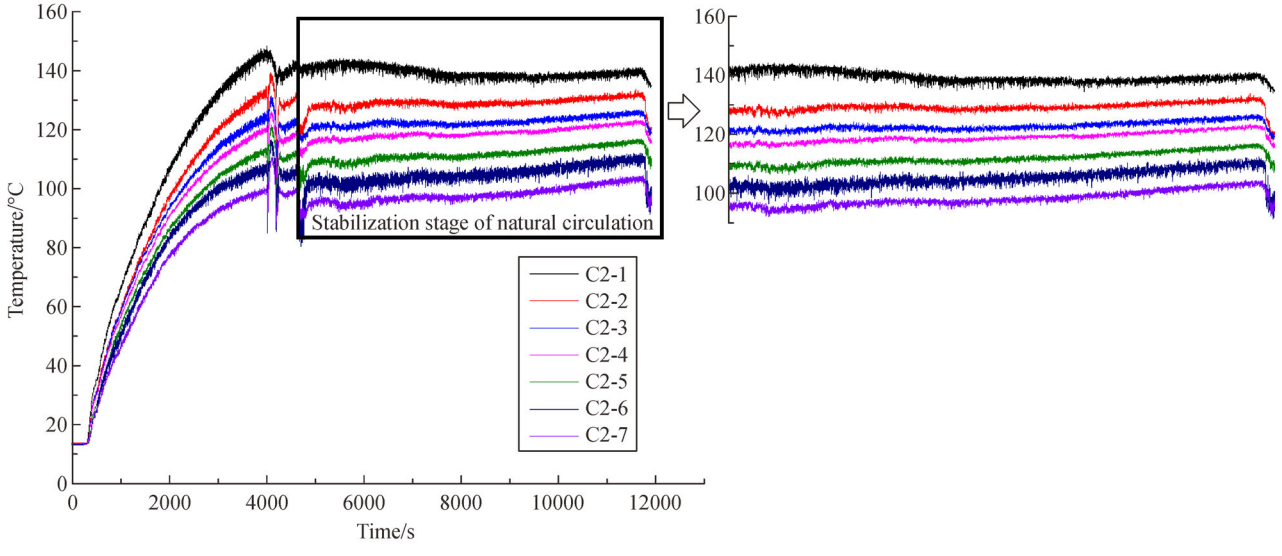

Fig. 5 Transient temperature variation in single tube.

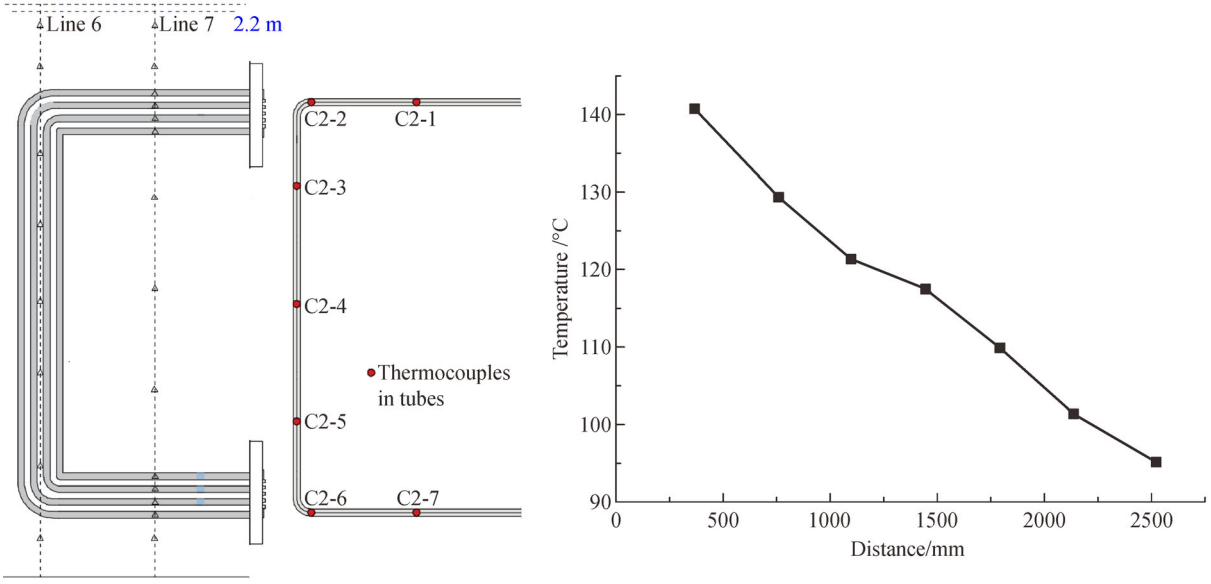

Fig. 6 Temperature distribution in tube (C2) at 6000 s.

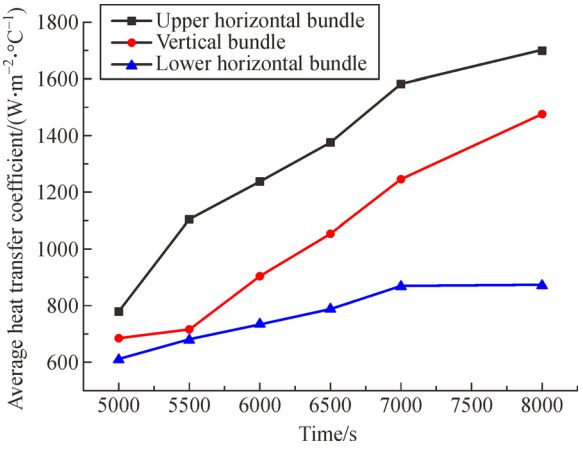

Fig. 7 Average heat transfer coefficient variation for different parts of C-shape tubes bundle.

3.2 Heat transfer characteristics analysis

In this paper, the average heat transfer coefficient variation for different parts of the C-shape tubes bundle is shown in Fig. 7, which confirms that the upper horizontal bundle has the best heat transfer effect due to the combination of the natural and forced convection on the outside wall at the beginning. Then, the nucleate pool boiling on the outside of the tubes occurs first in the upper bundle, which further enhances the heat transfer. For the vertical part, the average HTC increases fast as the test proceeds with the enhancement of the mixing effect under natural convection condition. However, the average HTC of the lower horizontal bundle remains relatively low for a very long time. The probably reason for this is that the fluid on the secondary side always remains inactive in the lower region, which is disadvantageous to heat transfer.

In the process of passive decay heat removal, the heat can be transferred from the primary side fluid to the secondary side fluid through the PRHR HX tubes. The main heat transfer mechanisms are single-phase forced convection on the PRHR HX tube inner side wall, conduction through the tube, and natural convection or nucleate boiling on the PRHR HX tube outer side wall in different stages. For the single-phase forced convection in the tube, the Dittus-Boelter correlation is applied for the calculation of the heat transfer coefficient of the inner surface of the tube [10]. The Dittus-Boelter correlation is given as

$$Nu_{\text{in}} = \frac{h_{\text{in}} d_{\text{in}}}{\lambda} = 0.023 Re^{0.8} Pr^{0.3}, \tag{1}$$

which is valid in the range of $Re = 10^4$–1.2×10^5, $Pr = 0.7$–120, and $l/d \geqslant 60$. Herein, Nu is Nusselt number and Re is the Reynolds number in the tube channel with the inner diameter as the characteristic length, and Pr is the Prandtl number of the fluid in the tube. Re is calculated by

$$Re = \frac{u d_{\text{in}}}{v} = \frac{(4W/(n\rho\pi d_{\text{in}}^2))d_{\text{in}}}{v}. \tag{2}$$

where u is the velocity, d_{in} is the inner diameter of the tube, v is the kinematic viscosity, W is the mass flow rate, n is the number of tubes in the bundle, ρ is the density.

As is shown in Fig. 8, each selected tube has seven temperature metrical points to obtain the temperature distribution and is divided into several cells through any two metrical points. Some important cells in the horizontal bundle and the vertical bundle are selected to analyze the

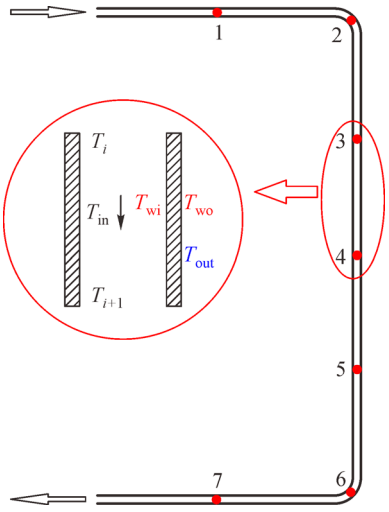

Fig. 8 Thermocouples arrangement of selected tubes.

heat transfer characteristics and each part of the cells is studied as a calculation unit. The fluid temperatures at the inlet and outlet of the calculation unit (T_i, T_{i+1}) are measured by the thermocouples arranged in the tube. The fluid temperature in the unit ($T_{in} = \frac{T_i + T_{i+1}}{2}$) is calculated as the characteristic value to get the fluid physical properties in the primary side. Based on the energy balance conservation and Dittus-Boelter correlation, the temperature of the outside wall (T_{wo}) and inner side wall (T_{wi}) are calculated as [11]

$$Q_i = \frac{T_{in} - T_{wi}}{R_{in}} = \frac{T_{wi} - T_{wo}}{R_w} = c_p W (T_i - T_{i+1}), \quad (3)$$

$$T_{wi} = \frac{(R_w \cdot T_{in} + R_{in} \cdot T_{wo})}{R_w + R_{in}}, \quad (4)$$

$$T_{wo} = T_{in} - c_p W (R_{in} + R_w)(T_i - T_{i+1}), \quad (5)$$

where R_{in} ($R_{in} = \frac{1}{h_{in} A_{in}} = \frac{1}{h_{in} \pi d_{in} l_i}$) represents inner tube thermal resistance and R_w ($R_w = \frac{\ln(d_{out} - d_{in})}{2\pi\lambda l_i}$) denotes tube wall heat conduction resistance.

The local average heat transfer coefficient in the secondary side h_{out} is calculated by

$$h_{out} = \frac{q}{T_{wo} - \overline{T}_{out}} = \frac{Nu \cdot \lambda}{D_h}, \quad (6)$$

where q is the heat flux on the outside wall, T_{wo} is the temperature of the outside wall which is obtained by Eq. (5), $\overline{T}_{out}$ is the corresponding average temperature of the fluid channels at the same height, λ is the thermal conductivity, and D_h is the characteristic length. In this paper, the local average heat transfer coefficients obtained by experiments are applied to verify the applicability of different correlations for this specific heat transfer condition.

In addition, the temperature of the outside wall T_{wo} and the onset boiling temperature T_{ONB} determine whether the heat transfer mechanism in the secondary side is single phase natural convection or subcooled/saturated nucleate pool boiling. Single phase natural convection only occurs on the tube outside wall when T_{wo} is less than T_{ONB} and the ONB temperature in the outside wall can be predicted by [12]

$$T_{ONB} = T_{sat} + 0.556 \left(\frac{556.3q}{p^{1.156}} \right)^{0.3538 p^{0.0234}}. \quad (7)$$

For the single-phase natural convection stage, Grashof number (Gr) which is deduced from the governing equation of natural convection heat transfer is very significant in the analysis of natural convection heat transfer behaviors, whose values can quantify the mutual influence of buoyant forces and viscous forces in the stage.

The Grashof number is usually expressed as $Gr = \frac{g\alpha\Delta T D_h^3}{\nu^2}$ in the traditional correlations [10]. Rayleigh number Ra ($Ra = Gr \cdot Pr$) which is a measure of the instability of the fluid in the velocity boundary layer under natural convection condition is simply defined as the product of Gr and Pr, and the Pr is defined as the ratio of momentum diffusivity to thermal diffusivity. The vertical bundle section comprises of 12 symmetric arranged slender vertical tubes satisfying the slenderness criterion $Gr^{\frac{1}{4}} \frac{D}{H} < 35$ [13], and the geometric parameters of the tube such as length, outside diameter should be considered in the heat transfer correlations.

The Churchill and Chu [14] correlation developed from an immerged vertical wall is widely used for the vertical part of the tube under natural convection condition. The correlation is valid in the range of $Ra > 10^{10}$, and can be expressed as

$$Nu = \left[0.825 + \frac{0.387 Ra^{\frac{1}{6}}}{\left[1 + \left(\frac{0.492}{Pr} \right)^{\frac{9}{16}} \right]^{\frac{8}{27}}} \right]^2. \quad (8)$$

McAdams [15] also recommended another heat transfer correlation for vertical flat wall as expressed in Eq. (9), which covers the range of $Gr > 10^9$.

$$Nu = 0.13 Ra^{1/3}. \quad (9)$$

Fujii correlation developed from single vertical cylinder considers the influence of viscosity at the bulk fluid

temperature (ν_∞) and the heating rod outside wall temperature (ν_{wo}), which is available for $Ra > 10^{10}$ and expressed as

$$Nu = 0.017Ra^{0.4}\left(\frac{\nu_\infty}{\nu_{wo}}\right)^{0.21}. \quad (10)$$

In the calculation of Ra within the vertical rods bundle, the mean value of the temperature on the outside wall T_{wo} and the average temperature of the fluid channels at the same height $\overline{T}_{out}$ is selected as the characteristic value to get the fluid physical properties. The Grashof number is defined as $Gr = \frac{g\beta\Delta TD_h^3}{\nu^2}$ in the calculation and the cylinder height in the vertical part is selected as the characteristic length. The comparison of the empirical correlations for the vertical condition and the measured Nu number is shown in Fig. 9. According to Fig. 9, the proposed correlations Eqs. (8)–(10) are in good agreement with the experimental data in the range of $5 \times 10^{12} < Ra < 10^{13}$. In the lower Ra range, the results calculated by the empirical correlations are slightly larger than the measured Nu number whereas the measured Nu number increases faster than the empirical correlations with the increase of Ra. This reveals that the buoyancy lift-up effects of different tubes have a little influence on each other in the lower Ra range. With the increase of Ra, the mixing effect of tubes becomes increasingly evident, leading to a better heat transfer coefficient. Based on the experimental data, the revised heat transfer correlation Eq. (11) for PRHR HX vertical bundle under natural convection condition is proposed.

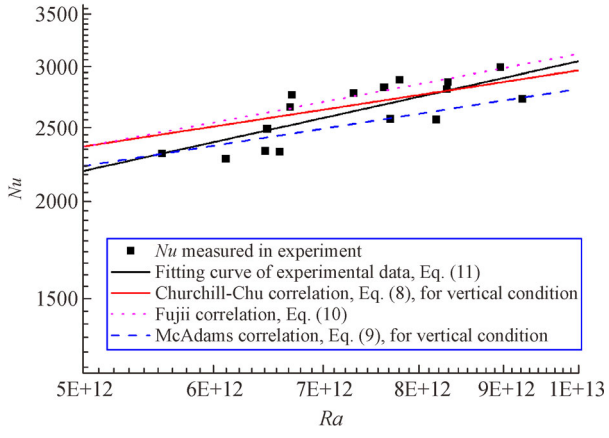

Fig. 9 Comparison of experimental data with traditional heat transfer correlations for the vertical bundle.

$$Nu = 0.00219Ra^{0.472}. \quad (11)$$

In the heat transfer process of C-shape tube bundle, the heat transfer mechanisms for the lower and upper horizontal bundles are not identical. For the lower section, the mechanism is typical natural convection, which is induced only by buoyancy occurring due to temperature gradients within the rods bundle. Churchill developed an empirical natural convection correlation for the horizontal cylinder with a uniform heat flux [16], expressed as

$$Nu = 0.579\frac{Ra^{0.25}}{[1+(0.442/Pr)^{9/16}]^{4/9}}. \quad (12)$$

McAdams proposed another free convection heat transfer correlation for the horizontal cylinder [15], expressed as

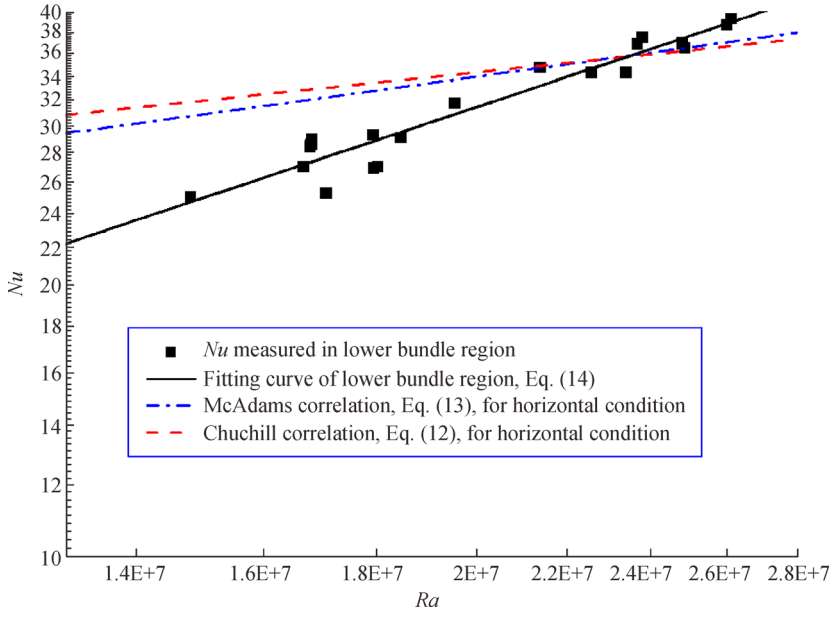

Fig. 10 Comparison of experimental data with traditional heat transfer correlations for the lower horizontal bundle.

$$Nu = 0.125Ra^{1/3}. \quad (13)$$

For the calculation of *Ra* number in the lower horizontal section, the outside diameter of the tubes is selected as the characteristic length and the expression of *Gr* is the same for the lower horizontal bundle and the vertical bundle. The measured *Nu* values within the lower horizontal bundle are compared with the predicted values calculated by the empirical correlations for the horizontal bundle, which can be seen from Fig. 10. In the lower *Ra* range, the measured *Nu* number is smaller than that predicted by traditional correlations. Then, it has a rapid growth and finally is larger than the predicted values with the increase of *Ra*. This reveals that the fluid surrounding the lower horizontal heating tubes remains almost inactive in the lower *Ra* range. Hot plume forms and hinders the heat from transferring out, weakening the heat transfer effect in natural convection. With the increase of *Ra*, the fluid surrounding the horizontal bundle become increasingly active to enhance the mixing effect, leading to a better heat transfer coefficient. The fitting curve of the experimental data are also shown in Fig. 10, which is expressed as

$$Nu = 3.99 \times 10^{-5} Ra^{0.807}. \quad (14)$$

For the upper horizontal bundle, the mechanism is the mixing of natural convection and forced convection due to the fluid heated flowed up by the lower horizontal bundle. In the mixed convection process, the heat transfer effect of the upper section is much stronger than that of the lower section and Richardson's number (*Ri*) is used to quantify the mutual effect of the natural and forced convection [17]. The heat transfer effect in this region is calculated by combining the calculation of two heat transfer mechanisms, which is elaborated in Ref. [5].

$$Ri = Gr/Re^2. \quad (15)$$

4 Conclusions

In this paper, an overall natural circulation loop facility including the simulator of the reactor core, a scaled-down IRWST, and a PRHR HX model which is simulated by 12 symmetric arranged C-shape tubes is constructed to investigate the overall and local hydraulic performance. It is also used to provide the experimental data for the verification of the existing system programs and the results are applied for the modification of the relative models in the system program. The main conclusions are summarized as follows.

The primary and secondary side coupling natural convection heat transfer characteristics of the PRHR HX are studied for the first time in this paper. The overall distribution of the average HTC for C-shape tubes bundle is obtained. The upper horizontal bundle has the best heat transfer coefficient due to its specific heat transfer mechanism. Meanwhile, the proposed correlations are in good agreement with the experimental data and the revised correlations for PRHR HX lower and vertical bundles under natural convection condition are developed.

The key thermal hydraulic characteristics of natural circulation in the primary side and natural convection in the large volume region are obtained. When natural convection occurs in the secondary side, the residual heat is removed to the IRWST steadily and thermal stratification forms in the vertical direction, whereas the temperature difference is not obvious in the lateral direction.

The heat transfer characteristics and correlations for the C-shape tube bundle designed for the PRHR HX in AP1000 are carefully evaluated and discussed. For the natural convection within the vertical bundle, the heat transfer condition is close to that of the vertical wall or single cylinder in the lower range of *Ra*. With the increase of *Ra*, the mixing effect becomes increasingly evident, causing the enhancement of the heat transfer.

For the natural convection within the lower horizontal bundle, the cases are also not identical for the lower and upper ranges of *Ra*. In the lower range of *Ra*, the flow pattern remains in the laminar state and the arrangement of tubes hinders the fluid surrounding the heating tubes from moving, weakening the heat transfer effect. With the increase of *Ra*, the mixing effect also plays an important role in the heat transfer process, leading to a better heat transfer coefficient.

Acknowledgements This work was supported by the National Science and Technology Major Project of China (Grant No. 2017ZX06004002-006-002) and the National Natural Science Foundation of China (Grant No. 51906069).

Notations

A	Area/m^2
c_p	Specific heat of constant pressure/($J \cdot kg^{-1} \cdot °C^{-1}$)
d	Diameter/m
D	Rod diameter/m
D_h	Hydraulic characteristic length/m
g	Gravitational acceleration/($m \cdot s^{-2}$)
Gr	Grashof number
h	Heat transfer coefficient/($W \cdot m^{-2} \cdot °C^{-1}$)
H	Height/m
l	Length/m
Nu	Nusselt number
n	Number of tubes in the bundle
p	Pressure/Pa
Pr	Prandtl number
Q	Total heat flux in energy balance equation/W
q	Heat flux/($W \cdot m^{-2}$)

Ra	Rayleigh number
Re	Reynolds number
Ri	Richardson number
T	Temperature/°C
u	Velocity/$(m\cdot s^{-1})$
W	Mass flow rate/$(kg\cdot s^{-1})$
x	Length along lateral direction/m
y	Length along wide direction/m
z	Length along height direction/m
Greek symbols	
Δ	Difference between two quantities
λ	Thermal conductivity/$(W\cdot m^{-1}\cdot °C^{-1})$
ρ	Density of fluid/$(kg\cdot m^{-3})$
α	Thermal expansion coefficient/$°C^{-1}$
v	Kinematic viscosity/$(m^2\cdot s^{-1})$
Subscripts	
in	Tube inner side
out	Tube outside
sat	Saturation
w	Wall
wo	Tube outside wall
wi	Tube inside wall
Abbreviations	
IRWST	In-containment refueling water storage tank
ONB	Onset of nucleate boiling
PRHR HX	Passive residual heat removal heat exchanger
HTC	Heat transfer coefficient
PRHRS	Passive residual heat removal system
RCS	Reactor coolant system

References

1. Lin C G. The Advanced Passive Pressurized Water Reactor AP1000. Beijing: Atomic Energy Press, 2008
2. Reyes J N. Final report of NRC AP600 research conducted at Oregon State University. NUREG/CR-6641, 1999
3. Yonomoto T, Kukita Y, Schultz R R. Heat transfer analysis of the passive residual heat removal system in ROSA/AP600 experiments. Nuclear Technology, 1998, 124(1): 18–30
4. Men Q M, Wang X S, Zhou X, et al. Heat transfer analysis of passive residual heat removal heat exchanger under natural convection condition in tank. Science and Technology of Nuclear Installations, 2014: 279791
5. Lu D G, Zhang Y H, Fu X L, et al. Experimental investigation on natural convection heat transfer characteristics of C-shape heating rods bundle used in PRHR HX. Annals of Nuclear Energy, 2016, 98: 226–238
6. Zhang Y H, Lu D G, Wang Z Y, et al. Experimental investigation on pool-boiling of C-shape heat exchanger bundle used in PRHR HX. Applied Thermal Engineering, 2017, 114: 186–195
7. Tao J Q, Gu H H, Xiong Z Q, et al. Investigation on transient thermal hydraulics of reduced scale passive residual heat removal heat exchanger in tank. Annals of Nuclear Energy, 2019, 130: 402–410
8. Liu Y B, Wang X S, Men Q M, et al. Heat transfer analysis of passive residual heat removal heat exchanger under tube outside boiling condition. Science and Technology of Nuclear Installations, 2017: 3497103
9. Kang M G. Experimental investigation of tube length effect on nucleate pool boiling heat transfer. Annals of Nuclear Energy, 1998, 25(4–5): 295–304
10. Yang S M, Tao W Q. Heat Transfer. Beijing: Higher Education Press, 2006 (in Chinese)
11. Zhang Y H, Yuan Y L, Feng L, et al. Application of the modified heat transfer formulas for the C-type heat exchanger in passive heat removal system of CAP1400. Applied Thermal Engineering, 2019, 159: 113876
12. Bergles A E, Rohsenow W M. The determination of forced-convection surface-boiling heat transfer. Journal of Heat Transfer, 1964, 86(3): 365–372
13. Popiel C O, Wojtkowiak J. Experiments on free convective heat transfer from side walls of a vertical square cylinder in air. Experimental Thermal and Fluid Science, 2004, 29(1): 1–8
14. Churchill S W, Chu H H S. Correlating equations for laminar and turbulent free convection from a vertical plate. Interactional Journal of Heat and Mass Transfer, 1975, 18(11): 1323–1329
15. McAdams W H. Heat Transmission. 3rd ed. New York: McGraw-Hill, 1954
16. Churchill S W. Laminar free convection from a horizontal cylinder with a uniform heat flux density. Letters in Heat and Mass Transfer, 1974, 1(2): 109–111
17. Ghiaasiaan S M. Convective Heat and Mass Transfer. New York: Cambridge University Press, 2011